

ARTICLE TYPE

HINORA II: Testing the Existence of the Council of Giants in Λ CDM simulations

Edward Olex,¹ Alexander Knebe,^{1,2,3} Noam I. Libeskind,⁴ Stefan Gottlöber,⁴ and Dmitry I. Makarov⁵¹Departamento de Física Teórica, Módulo 15, Facultad de Ciencias, Universidad Autónoma de Madrid, 28049 Madrid, Spain²Centro de Investigación Avanzada en Física Fundamental (CIAFF), Facultad de Ciencias, Universidad Autónoma de Madrid, 28049 Madrid, Spain³International Centre for Radio Astronomy Research, University of Western Australia, 35 Stirling Highway, Crawley, Western Australia 6009, Australia⁴Leibniz-Institut für Astrophysik Potsdam (AIP), An der Sternwarte 16, D-14482 Potsdam, Germany⁵Special Astrophysical Observatory, Russian Academy of Sciences, Nizhnii Arkhyz, 369167 Russia**Author for correspondence:** E. Olex, Email: edward.olex@uam.es.

Abstract

The discovery of the galaxy ring known as the Council of Giants (CoG) highlights the need to explain such structures in the Local Universe. In the first paper of this series we presented HINORA – a code to locate (ring-like) structures in 3D point sets – and used it to identify the CoG in the most complete observations of the Local Volume. Here, in Part II, we apply the same method to cosmological simulations to quantify the possible existence of such objects in the Λ CDM model of structure formation. We analyze DM-only simulations with random and constrained initial conditions, selecting regions that reproduce the properties of the Local Group and Volume, respectively. In order to use the same selection criteria as previously done for observations, we relate K-band luminosities to halo masses through semi-empirical relations. After confirming that the selected regions from the simulations match the observed mass function and density of the Local Universe, we use HINORA to search for ring-like structures in them. We find that the existence of CoGs in Λ CDM simulations is a rather unusual phenomenon. The observed CoG represents an anomaly of more than 2.7σ from what is expected in the distribution of massive galaxies in Λ CDM. These results hint that the CoG could either be a rare chance configuration or the imprint of physical processes at intermediate scales that standard DM-only simulations fail to capture.

Keywords: galaxies: haloes, Local Group, cosmology: theory, dark matter, large-scale structure

1. Introduction

The current era of astronomical surveys is revolutionizing our understanding of the Universe, revealing unprecedented details on both large and small scales. While redshift catalogs capture cosmic structures on vast scales, precise distance measures shed new light on the galaxies closest to the Milky Way (MW). In recent years, detailed analyses of distance and peculiar velocity catalogs in the Local Universe have uncovered hidden patterns in the distribution of galaxies, with important implications for modern cosmology. On small scales, attention has been drawn to the observation of kinematically stable satellite planes around the MW, Andromeda and also Centaurus A (see Bullock and Boylan-Kolchin 2017; Pawlowski 2018; Tully et al. 2015; Müller et al. 2018), which have been extensively studied in cosmological simulations (Libeskind et al. 2005; Libeskind et al. 2009; Lovell et al. 2011; Wang, Frenk, and Cooper 2013; Cautun et al. 2015), suggesting that their origin does not pose a major tension with the standard cosmological model (Buck, Macciò, and Dutton 2015; Gillet et al. 2015; Ahmed, Brooks, and Christensen 2017; Shao, Cautun, and Frenk 2019; Samuel et al. 2021; Pham, Kravtsov, and Manwadkar 2023; Gámez-Marín et al. 2024).

Flat structures are not limited to dwarf satellites. The massive galaxies within ~ 10 Mpc of the Milky Way, located in the so-called Local Volume (LV), form a flat arrangement (Rubin 1951; de Vaucouleurs 1953, 1958) known as the Local Sheet (Tully et al. 2008). Recently, Peebles (2023) pointed out that

extensive sheet-like structures appear more frequently than expected, highlighting the lack of a clear explanation within Λ CDM. Additional evidence suggests that Local Sheet-like structures are rarely reproduced in cosmological simulations (Neuzil, Mansfield, and Kravtsov 2020; Aragon-Calvo, Silk, and Neyrinck 2023), although constrained simulations appear more capable of generating such configurations (Sawala et al. 2024).

Our research focuses on studying these types of flat regular structures simultaneously in observations and simulations, with particular emphasis on one case: the ring of massive galaxies known as the Council of Giants (CoG), discovered by McCall (2014) in his dataset. In that paper, McCall argues that the CoG consists of 12 massive galaxies (10 of them spirals) forming a 3.75 Mpc ring-like structure embedded in the Local Sheet and containing the Local Group (LG) near its center.

In our first paper (Olex et al. 2024, from now on referred to as Paper I), we developed High-Noise RANSAC (HINORA), a method that enables the identification of regular patterns in galaxy catalogs from both observations and simulations. By applying HINORA to the updated Local Volume Galaxies survey (LVG; Karachentsev, Makarov, and Kaisina 2013), in Paper I we located the CoG in the regime of massive galaxies, as well as a second, similar ring within the LV when all luminosity regimes were considered. We also detected both patterns statistically by analyzing the clustering properties of the survey.

The existence of these galaxy rings in the LV could provide valuable insight into how the Local Sheet and the LG were formed, and perhaps even reveal new, still-unknown phenomena in the general process of structure formation at intermediate scales. However, their existence might also be the result of purely coincidental alignments created by random motions of nearby galaxies. This raises a fundamental question: are galaxy rings like the CoG signatures of new physics, or simply chance alignments? The present, second paper aims to shed light on this issue.

For this purpose, we have selected in cosmological dark matter (DM) only simulations environments analogous to that surrounding the LG. We extract the simulated LVs from two main types of simulations: those with random initial conditions and those with constrained phases – such as the HESTIA (Libeskind *et al.* 2020) produced by the CLUES collaboration^a – specifically designed to reproduce the cosmography near the LG. Both sets satisfy similarity criteria defined according to the known properties of the LV. Using halo luminosity–mass relations, we restrict the simulated objects to the massive regime where the observed CoG resides, and we apply the same HINORA analysis as was performed for the LVG. This enables us to quantify how often rings appear in the simulated LVs and to estimate the probability of their formation within Λ CDM.

This paper is structured as follows. Section 2 describes the cosmological simulations and our procedure to identify LV analogues in them. Section 3 summarises the observed properties of the CoG from Paper I and the simulation-to-observational mapping adopted by us. In Section 4 we compare the simulated LV realisations with the observed LVG catalogue. Section 5 presents the application of HINORA to search for CoG-like rings in those environments. We close with a brief discussion and conclusions in Section 6.

2. Local Volume simulations

The LV is, so far, the only region of the Universe in which a ~ 4 Mpc-radius ring of massive galaxies has been found. In Paper I, we used the LVG catalog to study this region of the Universe, which consists of 1069 galaxies within 10 Mpc of the MW. In this section, we present the different types of simulations we use to reproduce this environment and study the potential formation of CoGs in it.

2.1 Constrained simulations

To reproduce as closely as possible the observed cosmography of the LV, we use the HESTIA cosmological simulations (Libeskind *et al.* 2020) that are based upon constrained initial conditions. Simulations such as HESTIA and others carried out by the CLUES collaboration (Gottlöber, Hoffman, and Yepes 2010; Libeskind *et al.* 2010; Carlesi *et al.* 2016; Sorce *et al.* 2016) successfully generate environments that resemble both the LG (Libeskind *et al.* 2020) and the surrounding LV

(Wempe *et al.* 2025), by reconstructing the large-scale structure of the Local Universe. To do this, CLUES simulations use observables that allow the local density field to be reconstructed through a Wiener Filter, thereby obtaining constraints on the Gaussian field that generates the initial conditions (Hoffman and Ribak 1991; Zaroubi *et al.* 1995). See Hoffman (2009) for a more complete summary of this technique. In the case of HESTIA, the constrained initial conditions are based on the CosmicFlows-2 survey (CF2, Tully *et al.* 2013) using the observed galaxy positions and peculiar velocities.

Since these simulations do not constrain small scales (i.e. non-linear scales corresponding to the LG and below), several exploratory runs are required to reproduce the finer details of the LG. In practice, nearly 10^3 low-resolution constrained initial phases were first generated in periodic boxes of side $100 h^{-1}$ Mpc (147.5 Mpc assuming Planck Collaboration XVI (2014) based cosmology), each containing 256^3 DM particles. For each run, a Lagrangian region of radius $\simeq 14.7$ Mpc ($10 h^{-1}$ Mpc) that collapses to the LV at $z = 0$ was identified and re-simulated at high resolution following the prescription of Katz and White (1993), replacing the original particles with an effective resolution of 512^3 within the central sphere. This resolution is sufficient to resolve LG-like halos with several thousand particles.

The particular set used here consists of DM-only simulations of a “zoomed” sphere with radius $10 h^{-1}$ Mpc ($\simeq 14.7$ Mpc) and a mass resolution of $m_{\text{DM}} = 6 \times 10^8 M_{\odot}$, embedded in a periodic box of $100 h^{-1}$ Mpc. They were evolved with AREPO (Weinberger, Springel, and Pakmor 2020) using the Planck Collaboration XVI (2014) based cosmology $\Omega_m = 0.318$, $\Omega_b = 0.048$, $\Omega_{\Lambda} = 0.682$, $\sigma_8 = 0.83$, $n_s = 0.96$, and $h = 0.677$. Halos are identified with the AMIGA Halo Finder (AHF, Knollmann and Knebe 2009), using the M_{200} definition, i.e. the mass within a sphere of 200 times the critical density.

For the present work we start with selecting only those realisations that contain a pair of halos that satisfy the main properties of the LG based on the observed properties of the MW–M31 pair (see Section 3.2 of Libeskind *et al.* 2020).

We will refer to these properties as **HESTIA criteria**, and they are as follows:

- a) Two haloes of mass: $8 \times 10^{11} < M_{200}/M_{\odot} < 3 \times 10^{12}$.
- b) Separation: $0.5 < d_{\text{sep}}/\text{Mpc} < 1.2$.
- c) Isolation: no third halo more massive than the smaller one within 2 Mpc of the midpoint.
- d) Halo mass ratio of smaller to larger halo > 0.5 .
- e) Infalling, i.e. $v_{\text{rad}} < 0$.

The numerical values adopted for the HESTIA criteria are not meant to impose tight constraints on the detailed properties of the LG, but rather to define a broad observationally motivated window that selects plausible LG analogues. The adopted mass window reflects current observational estimates that place MW at about $1.0 - 2.1 \times 10^{12} M_{\odot}$ (Posti and Helmi 2019; Hartori *et al.* 2018; Monari *et al.* 2018; Watkins *et al.* 2019; Zaritsky and Courtois 2017) and M31 at about $0.6 - 2.0 \times 10^{12} M_{\odot}$ (Kaffe *et al.* 2018; Tamm *et al.* 2012; Diaz *et al.* 2014; Corbelli *et*

a. <https://www.clues-project.org/>

al. 2010). Similarly, the separation and kinematic ranges are chosen to encompass the current observational uncertainties on the MW-M31 system (see the discussion in Section 3.2 of Libeskind et al. 2020).

If the HESTIA criteria are met, the LG-like pair must be found within 5 Mpc of its expected position in the simulation, namely at the supergalactic origin: $(SGX, SGY, SGZ) = (0, 0, 0)$. No other cluster more massive than the simulated Virgo is allowed within a sphere of 20 Mpc centered on the LG^b. We note that the cluster selection has two complementary components. In all LV-like samples we impose a baseline requirement that no halo with $M_{200} > 2 \times 10^{13} M_{\odot}$ is present within the 10 Mpc LV, in order to exclude strongly cluster-dominated environments. In addition, the HESTIA constrained realizations are required to host a unique Virgo-like cluster at the observed CF2 position (~ 16 Mpc from MW, see Libeskind et al. 2020), reflecting the goal of reproducing the observed large-scale cosmography. After applying these criteria, a total of **64** different realizations of the LG are obtained, distinguished by the random-phase seeds that set their small-scale structure. As in our first work with the LVG survey, we restrict our analysis to galaxies within 10 Mpc of the candidate MW in each HESTIA simulation.

2.2 Random simulations

Given the success of the HESTIA simulations in reproducing various features of the Local Universe beyond the MW - Andromeda pair, we also adopt the same criteria to find LVs in random-type (i.e. unconstrained) simulations. To create a contrasting sample representative of a generic, unconstrained universe, we apply the five LG selection criteria to the Small MultiDark Planck simulation (SMD, Klypin et al. 2016). The SMD simulation is a $400 h^{-1}$ Mpc periodic box with a particle mass resolution of $m_{MD} = 9.6 \times 10^7 M_{\odot}$, evolved with GADGET-2 (Springel et al. 2005) under a Planck Collaboration XVI (2014) based cosmology of $\Omega_m = 0.307$, $\Omega_b = 0.048$, $\Omega_{\Lambda} = 0.693$, $\sigma_8 = 0.83$, $n_s = 0.96$, and $h = 0.678$. Halos are identified with the ROCKSTAR (Robust Overdensity Calculation using K-Space Topologically Adaptive Refinement) halo finder (Behroozi, Wechsler, and Wu 2013), using the M_{200} definition.

Once we locate LG-like galaxy pairs in SMD that satisfy all five criteria and the baseline cluster exclusion (i.e., no halos with $M_{200} > 2 \times 10^{13} M_{\odot}$ within 10 Mpc), we define their LVs as catalogs of all galaxies within 10 Mpc of the MW candidate (the less massive member of the LG pair). This procedure yields 4430 candidate volumes; after discarding those overlapping by more than 50% of their volume, we obtain a final set of **4048** independent LVs.

To test whether ring-like structures arise directly from intrinsic LV properties, we generate a third reference sample by placing 10^4 random spheres of radius 10 Mpc within the SMD box without any selection criteria, a number large enough to

^b. We also require a Virgo-like cluster (with a mass $> 2 \times 10^{14} M_{\odot}$) to be present, meaning that the constrained simulations must produce a cluster at the Virgo position. This is a relatively “light” criterion, as the constrained initial conditions algorithm nearly always forms a Virgo cluster.

provide a statistically representative sampling of the simulation volume. After excluding regions overlapping by more than 50%, this yields **9292** independent random LVs. Table 1 summarizes the three sets of simulated spherical volumes used in this work to search for possible galaxy rings.

Table 1. List of the simulated volumes in which we have searched for the Council of Giants using HINORA. Each volume consists of a sphere of radius 10 Mpc by similarity to LVG.

	HESTIA	SMD	SMD Random
Number	64	4048	9292
Simulation	HESTIA	Small MultiDark Planck	Small MultiDark Planck
Initial conditions	Constrained	Random	Random
Local Group	HESTIA criteria	HESTIA criteria	-
Exclude cluster environments	No LV halo with $M_{200} > 2 \times 10^{13} M_{\odot}$	No LV halo with $M_{200} > 2 \times 10^{13} M_{\odot}$	-
Virgo-like cluster at the CF2 position	Yes	-	-

All simulations employed here are DM-only and we restrict our analysis to masses well above the resolution limits. Two different halo finders are used: AHF for HESTIA and ROCKSTAR for SMD. The slight differences in Ω_m and h between HESTIA and SMD are likewise negligible for the scale studied.

3. Methodology

In this section we describe the approach used to search for CoG-like structures within our set of Λ CDM simulations. We first recall the observational definition of the CoG established in Paper I and describe how the HINORA algorithm identifies such ring-like systems. Next, we explain how observational quantities (K-band luminosities) are converted into DM halo properties to facilitate the comparison with simulated LVs.

3.1 The detection of the Council of Giants

We focus on the CoG-like ring identified in Paper I, found using HINORA in the regime of more massive galaxies, with luminosity cuts of $\log_{10}(L_K) > 9, 10, 10.5$, where L_K is the luminosity in the K-band. This structure, formed by the brightest galaxies in the LV, shows consistent properties across all cuts and exhibits the same geometrical features as the CoG reported by McCall (2014) (see Figs. 5 and 6 in Paper I).

The HINORA method used to identify the CoG in the LVG is based on the RANdom SAMple Consensus (RANSAC) algorithm, which applies a non-deterministic strategy to detect regular structures in point clouds. To find a ring-like pattern in the data, RANSAC randomly selects three points and defines the circle that passes through them, recording all points located

within a distance τ of that circle. The configuration that includes the largest number of points is then considered the best-fitting hypothesis. However, this approach has a key limitation: since it relies solely on maximizing the number of points, it will always identify a single structure even in a purely random distribution.

HINORA modifies RANSAC to overcome this issue by quantifying three properties of any detected structure using three new parameters:

- i) α , to quantify the noise in the data. This parameter is defined as the ratio $\alpha = N_I/(N_I + N_O)$ between the number of inliers N_I and outliers N_O associated with a given model. Its local value is compared with the global prediction $\bar{\alpha}$, which represents the expected value of α for the full dataset.
- ii) β , to quantify the regularity of the data. If ϕ_i denotes the angular separations between consecutive points along the detected ring, this parameter is defined as the ratio between the standard deviation σ_ϕ and the mean value $\langle\phi\rangle$ of these angles, $\beta = \sigma_\phi/\langle\phi\rangle$. Its value is compared with the global expectation $\bar{\beta}$ derived for the full dataset.
- iii) n_I , to quantify the overall statistical significance of the structure. It is defined as the fraction of inliers, $n_I = N_I/N_{\text{tot}}$, where N_{tot} is the total number of data points. This value is compared with the expected inlier fraction \bar{n}_I , which is fixed a priori.

Once the expected values of $\bar{\alpha}$ and $\bar{\beta}$ are computed analytically for a given dataset, and \bar{n}_I is specified, only structures satisfying $\alpha < \bar{\alpha}$, $\beta < \bar{\beta}$, and $n_I > \bar{n}_I$ are accepted. For a more detailed description of HINORA as well as the analytical prediction of $\bar{\alpha}$ and $\bar{\beta}$, see the Section 3 of Paper I.

HINORA depends on three parameters, which are set a priori rather than inferred from the data. In Paper I, these were defined as follows:

- a) τ , the allowed thickness of the ring. We adopt an inner radius of $\tau = 1$ Mpc.
- b) The minimum fraction of galaxies or halos that two detected rings must share in order to be considered the same structure. This prevents the method from identifying multiple slightly displaced copies of the same ring. We use a value of 30%.
- c) \bar{n}_I , as mentioned above the minimum fraction of the total galaxies or halos that a ring must contain to be accepted. We use $\bar{n}_I = 0.15, 0.20$, and 0.25 .

In this second paper, we keep the first two parameters fixed to the values adopted in Paper I, where they were shown to have no significant impact on the results, and vary only the third. The value of \bar{n}_I can strongly influence the identification of structures: low values may introduce spurious detections, while high values can suppress genuine ones (see Section 4 of Paper I). All other ring properties (e.g., radius, position, or orientation) are not imposed by the method but are directly inferred from the data. This is a key advantage of HINORA, as it avoids introducing biases in the geometry of the detected structures.

Table 2 lists the characteristics of the observed CoG obtained by applying HINORA to the unmodified LVG catalog.^c The geometrical parameters of the CoG remain remarkably stable across different luminosity cuts. We quantify this stability by measuring the maximum variation in three independent properties of the rings: the position of the center (in Mpc), the orientation angle between their planes (in degrees), and the radius (in Mpc), denoted as Δ_c , Δ_a , and Δ_r , respectively.

Table 2. Characteristics of the Council of Giants detected by HINORA in Paper I. The ‘‘SG’’ coordinates are in the Supergalactic reference system, while the orientation is normalized to 1.

	Coord.	Cut 1	Cut 2	Cut 3	Δ
$\log(L_k) >$		9	10	10.5	
$M_{200}/10^{11} M_\odot >$		1.01	2.84	6.06	
Center (Mpc)	SGX	-1.11	-0.35	-0.52	
	SGY	0.73	0.12	0.68	1.10
	SGZ	0.28	-0.22	-0.22	
Orientation	X	0.06	-0.06	-0.06	
	Y	0.01	-0.04	-0.02	7.24°
	Z	0.99	0.99	0.99	
Radius (Mpc)		4.35	3.83	3.76	0.59
Galaxies		26	10	9	
n_I		0.22	0.22	0.29	

These quantities express the maximum variation of the CoG geometry across luminosity cuts, and are used to identify as a single object a structure that appears in several mass-selected samples with slightly different positions, orientations, and sizes. For each geometric property, the Δ value corresponds to the maximum pairwise difference measured between the CoGs detected at different luminosity cuts. As shown in Table 2, the maximum displacement of the CoG center is $\Delta_c = 1.10$ Mpc, computed as the largest three-dimensional separation between any two centers listed in the table. Similarly, the maximum variation in orientation, $\Delta_a = 7.24^\circ$, corresponds to the largest angle between the planes defining the rings at different cuts, and the maximum change in radius is $\Delta_r = 0.59$ Mpc.

We adopt these maximum variations as tolerance thresholds when defining a CoG in the simulations, requiring that candidate rings exhibit the same or smaller level of geometric persistence (in all three parameters) across different mass cuts.

c. In Paper I, we modified the observational data to estimate the effect of distance uncertainties; see Section 4 of that paper for details.

3.2 Connecting simulations with observations

On the one hand we are dealing with observed properties like the K-band luminosity of galaxies, but on the other hand the simulations provide halo masses. In order to apply comparable cuts to the object properties, we convert the K-band luminosities used in Paper I into stellar masses (M_\star), and then relate those stellar masses to the halo masses (M_{200}) using semi-empirical relations. Infrared bands are best suited for this purpose because their M_\star/L relation is less sensitive to variations in stellar populations, age, star-formation history (SFH) and metallicity than in the optical bands (Röck et al. 2015; Wen et al. 2013; Meidt et al. 2014). In particular, the K-band provided by LVG is commonly used to estimate stellar mass: it suffers less dust extinction and is less affected by SFH (Bell et al. 2003; Brinchmann and Ellis 2000; Cole et al. 2001; Bundy, Ellis, and Conselice 2005; Taylor et al. 2011; Beare et al. 2019). We therefore use the K-band to estimate M_\star for LVG objects using several published relations, and subsequently derive their corresponding M_{200} mass. When an object lacks direct K-band data, we will adopt the K-band estimates provided by Karachentsev, Makarov, and Kaisina (2013), who derive them from other measured bands as described in their paper.

The empirical relation we use for the inference of the stellar mass is:

$$M_\star/L_K \sim 0.6M_\odot/L_\odot \quad (1)$$

demonstrated by McGaugh and Schombert (2014), and Lelli, McGaugh, and Schombert (2016); self-consistent with inference in other bands. None of the galaxies studied deviates more than $\sigma_{K \rightarrow \star} \sim 0.1$ dex from this color-independent function, which corrects the overestimation of stellar mass in K-band from previous constant relations by Bell et al. (2003) or Into and Portinari (2013) (Beare et al. 2019).

Once M_\star is estimated, we apply the semi-empirical stellar-halo mass relation (SHMR) of Rodríguez-Puebla et al. (2017) via abundance matching, with a scatter of less than $\sigma_{\star \rightarrow h} \sim 0.15$ dex. Specifically, we interpolate the tabulated numerical results for the mean inverted SHMR at $z = 0$ to determine the mean virial mass, M_h , for a given M_\star .

Since the SHMR contains the virial mass of the halo, we adopt

$$M_h \approx 1.22M_{200} \quad (2)$$

to convert between mass definitions, consistent with typical NFW concentration parameters for galaxies in this mass range (White 2001; Pierpaoli et al. 2003). Therefore we adopt an average conversion and account for the resulting uncertainty induced by the intrinsic scatter in the mass-concentration relation and by deviations from ideal NFW profiles. Recent studies that explicitly propagate these effects find a typical scatter of $\sigma_{h \rightarrow 200} \sim 0.1$ dex for mass conversions that do not assume an individual concentration value (Ragagnin et al. 2021; Diemer and Kravtsov 2015; Dutton and Macciò 2014).

This procedure yields estimates of the M_{200} values corresponding to the L_K luminosity cuts that define the CoG, with further details provided in the Appendix 1. The total scatter from the relation between K-band luminosity and M_{200} is

$$\sigma_{K \rightarrow 200}^2 \approx \sigma_{K \rightarrow \star}^2 + \sigma_{\star \rightarrow h}^2 + \sigma_{h \rightarrow 200}^2, \quad (3)$$

which results in $\sigma_{K \rightarrow 200} \sim 0.2$.

4. Local Volume properties

The M_{200} estimates enable a direct comparison between the DM halos in the simulations and the galaxies observed in the LVG. To examine possible differences in their mass distributions, Fig. 1 shows the cumulative halo mass function (CHMF) for all LVs identified in the HESTIA (solid blue line) and SMD (dashed red line) simulations. The shaded regions indicate the $\pm 1\sigma$ scatter around the mean. Randomly placed spherical volumes within the SMD box (dotted green line) are also shown for reference. As these random volumes are unconstrained, they exhibit a much larger intrinsic scatter. Both HESTIA and SMD LVs display systematically higher halo abundances than random volumes, as expected since the LG forms in a relatively dense region of the cosmic web (Forero-Romero and González 2015). Vertical lines indicate the M_{200} thresholds corresponding to the luminosity cuts where the CoG was identified in Paper I (see Table 2).

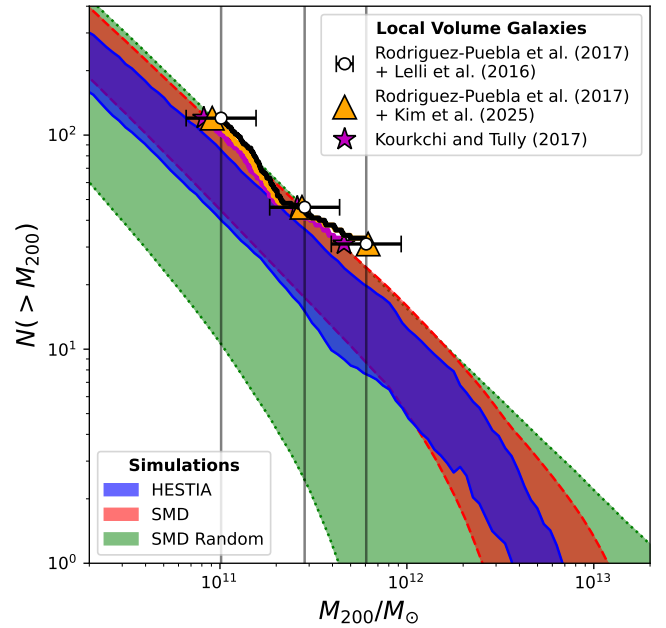


Figure 1. Cumulative halo mass function for M_{200} in each of the Local Volumes extracted from the HESTIA constrained simulations (blue region) and SMD random simulation (red region). Also shown in green are randomly placed volumes in SMD. The simulations are compared with those obtained for the LVG survey using three different M_h/L_k relations. The vertical lines indicate the main mass cuts at which HINORA was applied in Sec. 5.

Figure 1 also includes the observed halo abundance in the LVG, derived using the Lelli, McGaugh, and Schombert (2016) and Rodríguez-Puebla et al. (2017) relations (L+RP) discussed earlier with the total scatter represented by the error bars. For comparison, two additional conversions between L_K and M_{200} were tested. The first combines Kim et al. (2025) with Rodríguez-Puebla et al. (2017) (K+RP), using synthetic spectral energy distributions to estimate M_\star/L_K . The second, from

Kourkchi and Tully (2017) (KT), provides a direct relation between $\log(M_h/L_K)$ and has been applied previously to LVG analyses of satellite kinematics (Karachentsev and Kashibadze 2021). Details of these conversions and their implementation are given in Appendix 1. We find that the systematic differences among the three relations (L+RP, K+RP, and KT) are consistently smaller than the intrinsic scatter of L+RP, which we therefore adopt as our fiducial relation and reference uncertainty. The most notable result is the systematic excess of massive halos in the LVG compared to the simulated LV-like environments, particularly in the CoG mass regime. A similar excess relative to Λ CDM expectations has been reported previously using B-band luminosities in the LVG (Neuzil, Mansfield, and Kravtsov 2020).

Another key property that characterizes the LV environment is its matter density. To assess this, we compute for each LV the halo density contrast relative to the cosmic mean. We define ρ_h as the sum of the masses of halos with $M_{200} > 10^{11} M_\odot$ (or equivalently $L_K > 10^9 L_\odot$) divided by the LV volume, $V = (4/3)\pi(10\text{Mpc})^3$:

$$\rho_h = \sum_i \frac{M_{200}^i}{V}; \quad M_{200}^i > 10^{11} M_\odot \quad (4)$$

The mean background halo density, $\bar{\rho}_h$, is obtained by summing all halos with $M_{200} > 10^{11} M_\odot$ in the full SMD simulation and dividing by its total volume $(590\text{Mpc})^3$. The halo density contrast for each LV is then

$$\delta_h = \frac{\rho_h - \bar{\rho}_h}{\bar{\rho}_h} \quad (5)$$

which, as in the standard definition, distinguishes overdense regions ($\delta_h > 0$) from underdense ones ($\delta_h < 0$).

Figure 2 shows the probability distribution function (PDF) of $1 + \delta_h$ for the LVs identified in HESTIA and SMD. Observational results from LVG using the L+RP relation are also included for comparison (black line + gray area). The randomly placed spherical volumes exhibit large variations in total mass, ranging from nearly empty voids to dense clusters within the SMD box. In contrast, the constrained HESTIA and LG-like SMD volumes tend to occupy intermediate-density environments, highlighting the particular cosmographic conditions of the LG. A mild excess in halo mass within the LVG, already apparent in the CHMF, is again visible in this distribution.

These results indicate that the simulated LVs reproduce environments broadly comparable to that of the LVG, showing only a mild excess of mass, consistent with previous findings for the LG in cosmological simulations. The next step is to investigate whether CoG-like structures can naturally emerge within such environments, and, if they do, to determine how frequently they occur.

5. The Council of Giants in Λ CDM

When eventually applying HINORA to our suite of simulations, any ring accepted in a single mass cut is treated as a

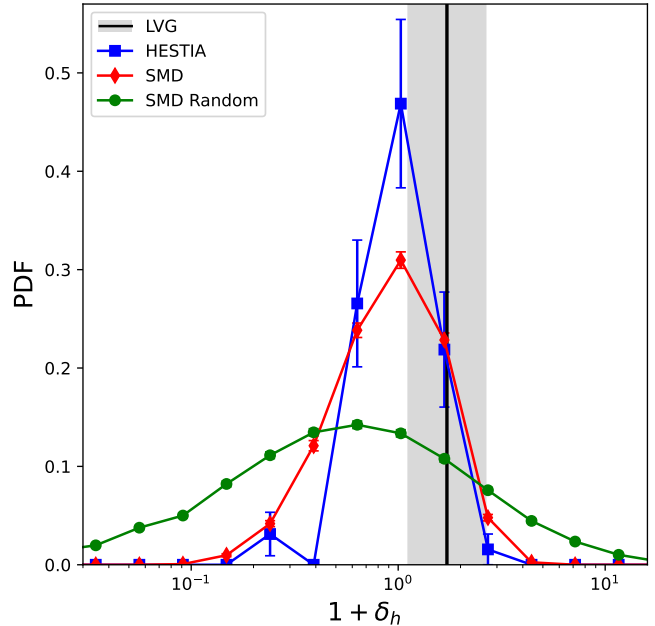


Figure 2. Probability distribution of the halo density contrast (defined in equation 10) for different Local Volumes. The different colors show the LVs obtained in HESTIA following all criteria (blue), SMD with all criteria (red), and SMD without any criteria (green). Value calculated for LVG survey and its associated scatter are shown with the black line + gray region.

“candidate”^d and then enters a second filtering stage. In that stage we require a candidate to be detected in all three mass cuts, and to satisfy the persistence thresholds Δ_c , Δ_d , and Δ_r defined in Section 3.1. For the simulated volumes we adopt the same set of HINORA parameters used for the LVG catalog in Paper I, increasing the number of iterations N by a factor of ten to improve convergence.^e

As laid out in Sec. 3.1, we also explore three values of the minimum halo fraction that define an accepted ring, $\bar{n}_l = 0.15, 0.20, 0.25$, which we use to classify a statistical detection as *weak*, *moderate* or *strong*, respectively. Note that the CoG is detected in the observations at $\bar{n}_l = 0.20$ (moderate presence), since $n_l > 0.20$ in all luminosity cuts (see Table 2). After applying HINORA, the detection rate is computed as the number of volumes with a detected ring divided by the total number of volumes. This ratio is plotted in Fig. 3, for the three choices of \bar{n}_l . While the bar represents the central value for mass cuts calculated with L+RP, the error bars are obtained by repeating the process for mass cuts shifted by the total scatter $\pm\sigma_{K \rightarrow 200}$.

We did not find any LV with more than one ring in any sample. The main feature of Fig. 3 is the low detection rate (below $\sim 5\%$ in all cases), which indicates that reproducing a structure with the geometry of the CoG is unlikely in the Λ CDM simulations we tested. The most optimistic case (3.12%) occurs in the HESTIA sample, suggesting that constrained ini-

d. Since we work in a regime of massive galaxies, some mass cuts (and some LVs) may contain very few objects, so small values of \bar{n}_l can produce spurious detections with only a few halos. To reduce false positives, we discard any accepted candidate with fewer than 8 inliers.

e. See equation (1) of Paper I.

tial phases slightly favour the appearance of CoG-like rings. However, this higher rate is attained only for weak rings; more significant (moderate or strong) structures are absent. Lower detection rates are found in the SMD sample and in the randomly placed volumes, the latter containing the fewest rings. The systematic difference between SMD and the random sample across all ring types points to an influence of the LG-selection criteria on the incidence of CoG-like structures. Moreover, because underdense regions occupy most of the simulated volume, the random spheres are predominantly located in such environments, which naturally explains their very low CoG detection rate.

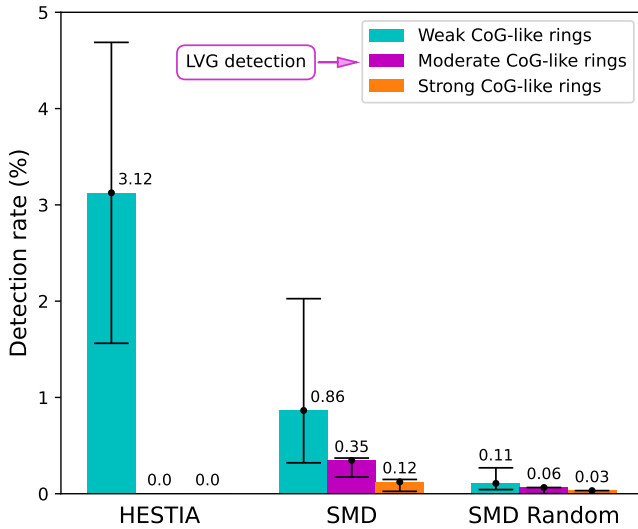


Figure 3. Fraction of galaxy rings detected in the different sets of simulated Local Volumes. The statistical strength of each detection fraction is classified as *weak*, *moderate*, or *strong* according to the minimum fraction of halos in the volume that belong to the ring, requiring $n_l > 0.15$, $n_l > 0.20$, and $n_l > 0.25$, respectively. The error bars consider the total uncertainty in the $L_K \rightarrow M_{200}$ relation.

5.1 Rings in random vs constrained initial conditions

Table 3 gives the number of volumes of each type that contain a ring (without considering the scatter) under the condition $n_l > \bar{n}_l$. For $\bar{n}_l = 0.15$, 35 confirmed rings are obtained in selected LVs of SMD. This implies that for a random draw of 64 LVs from SMD, the mean number of LVs with ring is 0.55, so the weak-ring detection in HESTIA is about $2/0.55 \approx 3.6$ times more favorable than in SMD with LG criteria, and 28.5 times more favorable than in random volumes.

To enable a proper comparison between simulations with constrained and random initial conditions without considering the scatter, we repeat the procedure of drawing 64 random SMD samples multiple times and computing the mean and standard deviation of the number of detected rings. This can be calculated analytically if the number of rings is treated as a random variable x of a hypergeometric distribution with mean $E[x]$:

$$E[x] = \frac{n_s k}{N} \quad (6)$$

Table 3. Rings detected by HINORA in the three simulated samples used in this work, as well as the expected average number of rings $E[x]$ from 64 random draws from each sample.

	HESTIA	SMD	SMD Random
Number of volumes	64	4048	9292
Rings found by HINORA			
Weak $\bar{n}_l = 0.15$	2	35	10
Moderate $\bar{n}_l = 0.20$	0	14	6
Strong $\bar{n}_l = 0.25$	0	5	3
$E[x]$			
Weak $\bar{n}_l = 0.15$	2	0.55 ± 0.73	0.07 ± 0.26
Moderate $\bar{n}_l = 0.20$	0	0.22 ± 0.47	0.04 ± 0.20
Strong $\bar{n}_l = 0.25$	0	0.08 ± 0.28	0.02 ± 0.14

where for comparison with HESTIA we set the number of samples $n_s = 64$. k is the number of LVs with ring found, while N is the total number of LVs in each case. The variance of the distribution is:

$$\sigma^2[x] = n_s \frac{N - n_s}{N - 1} \frac{k}{N} \frac{N - k}{N} \quad (7)$$

Table 3 contains $E[x]$ for each LV type and each value of \bar{n}_l , with the error representing the standard deviation calculated with the equation (7). Given the small counts involved, Poisson (counting) uncertainties are large and these factors should be taken as indicative. Note that in less optimistic scenarios, i.e. $\bar{n}_l = 0.20$ and $\bar{n}_l = 0.25$, HESTIA contains no rings, which means that the probability has to be at least less than $100/64 \approx 1.56\%$. The hypergeometric mean of SMD in the $n_l = 0.20$ case is 0.22, so a null result in HESTIA is compatible with the order of magnitude in which it differs from SMD since $0.22 \times 3.6 < 1$.

5.2 The significance of the Council of Giants detection

Under the null hypothesis that the observed LV is drawn from the same population as the simulated volumes, the per-volume detection probability estimated from the simulations is $p = k/N$. With a single observed LV in which the CoG is detected ($N = 1$, $k = 1$), the one-sided p -value for observing at least one CoG equals $p_{\text{val}} = p$, and the equivalent Gaussian significance is

$$z = \Phi^{-1}(1 - p_{\text{val}}). \quad (8)$$

where Φ is the Cumulative Distribution Function (CDF) of a normal distribution. Using the empirical frequencies measured in the three simulation sets, we obtain the z -score values shown in Table 4. The range of values takes into account the $\pm \sigma_{K \rightarrow 200}$ region within the total scatter of the L+RP relation.

Table 4 reports the significance of the deviation between the observed CoG in LVG and the null hypothesis based on

Table 4. Deviation in units of standard deviation (σ) between the LVG detection and Λ CDM predictions. Intervals denote the range of significance when considering model-dependent systematic errors.

	HESTIA	SMD	SMD Random
Weak $\bar{n}_l = 0.15$	1.69-2.16 σ	2.05-2.73 σ	2.78-3.33 σ
Moderate $\bar{n}_l = 0.20$	-	2.68-2.92 σ	3.22-3.70 σ

our simulated samples. The presence of a weak CoG-like ring in LVG corresponds to a $\geq 2.78\sigma$ anomaly relative to randomly chosen volumes, but this tension decreases to $\geq 2.05\sigma$ when comparing with volumes that contain an LG-like system, and falls to $\geq 1.69\sigma$ for volumes drawn from simulations with constrained initial conditions. In all cases, tension decreases as we reduce the effect of cosmic variance.

In the case where CoG has a moderate statistical presence, similar to the detection in LVG, the tension is greater: adopting the SMD sample restricted to LG-like environments as a realistic analogue of the observed LV yields a deviation of $\geq 2.7\sigma$ from the Λ CDM expectation.

6. Discussion and conclusions

To determine whether Council of Giants (CoG) formation is possible in the Λ CDM model, we compared the observed Local Volume Galaxy survey (LVG) with its analogues extracted from two types of cosmological simulations: the Small MultiDark (SMD), based on random initial conditions and representative of the average cosmic environment, and the HESTIA simulations, which use constrained initial conditions to reproduce the large-scale structure of the Local Universe. In Paper I, we introduced the HINORA algorithm to identify generic ring-like configurations in point distributions and confirmed the presence of the CoG in the LVG. Here, we extend that analysis to examine how frequently similar ring structures arise within these simulated reproductions of the Local Universe.

The simulated regions analysed in this work were selected to reproduce environments consistent with the observed Local Volume (LV). Using the known properties of the Local Group (LG) and the Virgo cluster as selection criteria, we identified 64 realisations from the HESTIA suite that successfully reproduce the local cosmography. Applying the same criteria to the SMD simulation yielded about four thousand comparable regions. The cumulative halo mass functions (CHMFs) of these samples show that both SMD and HESTIA reproduce the overall halo abundance observed in the LVG, although the observational data reveal a modest excess in the CoG mass regime ($M_{200} \sim 10^{11-12} M_{\odot}$). A similar trend is seen in the halo density contrast, with simulated LVs appearing slightly overdense relative to the cosmic background, consistent with the LG residing in an intermediate-density environment. These results confirm that our simulated volumes provide a realistic representation of the LV, yet they also suggest that the observed region is somewhat richer in massive halos than typical Λ CDM counterparts.

Using HINORA on the simulated samples, we recorded how many volumes contain a CoG-like ring with weak, moderate (i.e. comparable to the observation) or strong statistical presence, described by different values of the minimum halo fraction. Our main result is that CoG-like structures are very rare in the explored Λ CDM realisations, regardless of the detection threshold. Detection rates differ by more than an order of magnitude between the simulation sets, which provides useful information on the environmental mechanisms that can favour the appearance of such rings. In particular, when volumes are drawn completely at random from the SMD simulation box the probability of finding a CoG-like ring is very low (of order $\lesssim 0.2\%$ depending on the presence threshold). Imposing LG-selection criteria in SMD increases the frequency to $\lesssim 2\%$, while restricting the large-scale modes to match CosmicFlows-2 constraints (HESTIA) raises the weak-ring frequency further (up to $\sim 5\%$). However, the HESTIA constrained simulations do not reproduce a CoG with a statistical presence comparable to that observed in the LVG, although the appearance of CoG-like structures is slightly favoured in HESTIA compared to purely random realizations. With new observational data (Tully *et al.* 2023) and improved algorithms for constructing constrained simulations (Valade *et al.* 2026), it will be possible to test again whether the observed velocity field predicts not only the Virgo cluster, the LG, and the Local Void, but also the CoG. Such a result would support the interpretation that the CoG is inherent to the specific environmental conditions of the LG.

Adopting the SMD sample restricted to LG-like environments as a conservative Λ CDM null hypothesis, the observed CoG in LVG departs from the model expectation at the level of $> 2.7\sigma$. This level of tension indicates that, under the assumptions and detection criteria adopted in this work, the Local Universe is atypical compared to the ensemble of simulated MW-Andromeda regions, placing our galactic environment within the rare $\sim 0.35\%$ of volumes that host a CoG-like ring.

Although this tension is mild, we can consider two possible solutions to this disagreement. The first is to attribute the existence of the CoG to chance. This perspective is fully valid, although future studies are still required to better determine the probability of CoG formation. In the present investigation we have focused on the geometrical properties that define the ring structure of the CoG, as well as on the mass of the galaxies that compose it. However, there are additional properties reported by McCall (2014) that make the CoG special. Among them, the original paper points out that a large fraction of its galaxies are spirals, with only two being elliptical. Furthermore, based on the peculiar velocity dispersion, McCall (2014) shows that the CoG appears to be a dynamically stable structure, as a typical member would require about 9.6 Gyr to leave the Local Sheet. Specifying these additional properties in the observations and considering them in (hydrodynamic) simulations could improve the probability estimation of CoG formation.

A second possible explanation for the tension, which should be interpreted with caution, is that the formation of the CoG involves physical processes not captured by our cosmological

Λ CDM simulations. Exploring hydrodynamic simulations could reveal whether this issue is related to baryonic matter interactions. The standard cosmological model, in the absence of hydrodynamical processes, does not include any known mechanisms capable of generating a ~ 3.5 Mpc radius matter ring or the Local Sheet in which it resides (Peebles 2023), so exploring models that might alleviate this tension is desirable. Alternative scenarios that can produce flat structures include topological defects that favor the emergence of Local Sheet-like configurations, such as cosmic strings (Peebles 2023) or the (a)symmetron (Christiansen, Hassani, and Mota 2024). Investigating these and other possible extensions of Λ CDM could help clarify the origin of the tension associated with the existence of the CoG.

Acknowledgement

All authors thank the referee for their constructive comments that helped to improve the paper. EO thanks Daniel Ceverino for his advice and Sabina Olex for her perseverance. AK likes to thank Sonic Youth for daydream nation.

Funding Statement EO and AK are supported by the Ministerio de Ciencia e Innovación (MICINN) under research grant PID2021-122603NB-C21 as well as project PID2024-156100NB-C21 financed by MICIU /AEI/10.13039/501100011033/ FEDER, UE. EO received predoctoral fellowship from MICINN (FPI program, Ref. PRE2022-102254) The authors gratefully acknowledge the Gauss Centre for Supercomputing e.V for funding this project by providing computing time on the GCS Supercomputer SuperMUC-NG at Leibniz Supercomputing Centre.

Data Availability Statement The CosmoSim data base provides access to the SMD simulation and the Rockstar halo data. The data base is a service by the Leibniz Institute for Astrophysics Potsdam (AIP).

References

- Ahmed, Sheehan H., Alyson M. Brooks, and Charlotte R. Christensen. 2017. The role of baryons in creating statistically significant planes of satellites around Milky Way-mass galaxies. *MNRAS* 466, no. 3 (April): 3119–3132. <https://doi.org/10.1093/mnras/stw3271>. arXiv: 1610.03077 [astro-ph.GA].
- Aragon-Calvo, M. A., Joseph Silk, and Mark Neyrinck. 2023. The unusual Milky Way-local sheet system: implications for spin strength and alignment. *MNRAS* 520, no. 1 (March): L28–L32. <https://doi.org/10.1093/mnras/slac161>. arXiv: 2208.03338 [astro-ph.GA].
- Beare, Richard, Michael J. I. Brown, Kevin Pimbblet, and Edward N. Taylor. 2019. Evolution of the stellar mass function and infrared luminosity function of galaxies since $z=1.2$. *The Astrophysical Journal* 873, no. 1 (March): 78. <https://doi.org/10.3847/1538-4357/ab041a>. <https://dx.doi.org/10.3847/1538-4357/ab041a>.
- Behroozi, Peter S., Risa H. Wechsler, and Hao-Yi Wu. 2013. The ROCKSTAR Phase-space Temporal Halo Finder and the Velocity Offsets of Cluster Cores. *ApJ* 762, no. 2 (January): 109. <https://doi.org/10.1088/0004-637X/762/2/109>. arXiv: 1110.4372 [astro-ph.CO].
- Bell, Eric F., Daniel H. McIntosh, Neal Katz, and Martin D. Weinberg. 2003. The optical and near-infrared properties of galaxies. i. luminosity and stellar mass functions. *The Astrophysical Journal Supplement Series* 149, no. 2 (December): 289. <https://doi.org/10.1086/378847>. <https://dx.doi.org/10.1086/378847>.
- Brinchmann, Jarle, and Richard S. Ellis. 2000. The Mass Assembly and Star Formation Characteristics of Field Galaxies of Known Morphology. *APJL* 536, no. 2 (June): L77–L80. <https://doi.org/10.1086/312738>. arXiv: astro-ph/0005120 [astro-ph].
- Buck, Tobias, Andrea V. Macciò, and Aaron A. Dutton. 2015. Evidence for Early Filamentary Accretion from the Andromeda Galaxy's Thin Plane of Satellites. *APJ* 809, no. 1 (August): 49. <https://doi.org/10.1088/0004-637X/809/1/49>. arXiv: 1504.05193 [astro-ph.GA].
- Bullock, James S., and Michael Boylan-Kolchin. 2017. Small-scale challenges to the Λ cdm paradigm. *Annual Review of Astronomy and Astrophysics* 55 (1): 343–387. <https://doi.org/10.1146/annurev-astro-091916-055313>. eprint: <https://doi.org/10.1146/annurev-astro-091916-055313>. <https://doi.org/10.1146/annurev-astro-091916-055313>.
- Bundy, Kevin, Richard S. Ellis, and Christopher J. Conselice. 2005. The Mass Assembly Histories of Galaxies of Various Morphologies in the GOODS Fields. *APJ* 625, no. 2 (June): 621–632. <https://doi.org/10.1086/429549>. arXiv: astro-ph/0502204 [astro-ph].
- Carlesi, Edoardo, Jenny G. Sorce, Yehuda Hoffman, Stefan Gottlöber, Gustavo Yepes, Noam I. Libeskind, Sergey V. Pilipenko, et al. 2016. Constrained Local UniversE Simulations: a Local Group factory. *MNRAS* 458, no. 1 (May): 900–911. <https://doi.org/10.1093/mnras/stw357>. arXiv: 1602.03919 [astro-ph.CO].
- Cautun, Marius, Sownak Bose, Carlos S. Frenk, Qi Guo, Jiaxin Han, Wojciech A. Hellwing, Till Sawala, and Wenting Wang. 2015. Planes of satellite galaxies: when exceptions are the rule. *MNRAS* 452, no. 4 (October): 3838–3852. <https://doi.org/10.1093/mnras/stv1557>. arXiv: 1506.04151 [astro-ph.GA].
- Christiansen, Øyvind, Farbod Hassani, and David F. Mota. 2024. Asimulation: Domain formation and impact on observables in resolved cosmological simulations of the (a)symmetron. *A&A* 689 (September): A6. <https://doi.org/10.1051/0004-6361/202449188>. arXiv: 2401.02410 [astro-ph.CO].
- Cole, Shaun, Peder Norberg, Carlton M. Baugh, Carlos S. Frenk, Joss Bland-Hawthorn, Terry Bridges, Russell Cannon, et al. 2001. The 2dF galaxy redshift survey: near-infrared galaxy luminosity functions. *MNRAS* 326, no. 1 (September): 255–273. <https://doi.org/10.1046/j.1365-8711.2001.04591.x>. arXiv: astro-ph/0012429 [astro-ph].
- Corbelli, E., S. Lorenzoni, R. Walterbos, R. Braun, and D. Thilker. 2010. A wide-field H I mosaic of Messier 31. II. The disk warp, rotation, and the dark matter halo. *A&A* 511 (February): A89. <https://doi.org/10.1051/0004-6361/200913297>. arXiv: 0912.4133 [astro-ph.CO].
- de Vaucouleurs, Gerard. 1953. Evidence for a local supergalaxy. *AJ* 58 (February): 30. <https://doi.org/10.1086/106805>.
- . 1958. Further evidence for a local super-cluster of galaxies: rotation and expansion. *AJ* 63 (July): 253. <https://doi.org/10.1086/107742>.
- Diaz, J. D., S. E. Kposov, M. Irwin, V. Belokurov, and N. W. Evans. 2014. Balancing mass and momentum in the Local Group. *MNRAS* 443, no. 2 (September): 1688–1703. <https://doi.org/10.1093/mnras/stu1210>. arXiv: 1405.3662 [astro-ph.GA].
- Diemer, Benedikt, and Andrey V. Kravtsov. 2015. A Universal Model for Halo Concentrations. *ApJ* 799, no. 1 (January): 108. <https://doi.org/10.1088/0004-637X/799/1/108>. arXiv: 1407.4730 [astro-ph.CO].
- Dutton, Aaron A., and Andrea V. Macciò. 2014. Cold dark matter haloes in the Planck era: evolution of structural parameters for Einasto and NFW profiles. *MNRAS* 441, no. 4 (July): 3359–3374. <https://doi.org/10.1093/mnras/stu742>. arXiv: 1402.7073 [astro-ph.CO].

- Forero-Romero, J. E., and R. González. 2015. The Local Group in the Cosmic Web. *ApJ* 799, no. 1 (January): 45. <https://doi.org/10.1088/0004-637X/799/1/45>. arXiv: 1408.3166 [astro-ph.CO].
- Gómez-Marín, Matías, Isabel Santos-Santos, Rosa Domínguez-Tenreiro, Susana E. Pedrosa, Patricia B. Tissera, M. Ángeles Gómez-Flechoso, and Héctor Artal. 2024. The Origin of Kinematically Persistent Planes of Satellites as Driven by the Early Evolution of the Cosmic Web in Λ CDM. *APJ* 965, no. 2 (April): 154. <https://doi.org/10.3847/1538-4357/ad27da>. arXiv: 2402.03288 [astro-ph.GA].
- Gillet, N., P. Ocvirk, D. Aubert, A. Knebe, N. Libeskind, G. Yepes, S. Gottlöber, and Y. Hoffman. 2015. Vast Planes of Satellites in a High-resolution Simulation of the Local Group: Comparison to Andromeda. *APJ* 800, no. 1 (February): 34. <https://doi.org/10.1088/0004-637X/800/1/34>. arXiv: 1412.3110 [astro-ph.GA].
- Gottlöber, Stefan, Yehuda Hoffman, and Gustavo Yepes. 2010. Constrained Local Universe Simulations (CLUES). *arXiv e-prints* (May): arXiv:1005.2687. <https://doi.org/10.48550/arXiv.1005.2687>. arXiv: 1005.2687 [astro-ph.CO].
- Hattori, Kohei, Monica Valluri, Eric F. Bell, and Ian U. Roederer. 2018. Old, Metal-poor Extreme Velocity Stars in the Solar Neighborhood. *ApJ* 866, no. 2 (October): 121. <https://doi.org/10.3847/1538-4357/aaede5>. arXiv: 1805.03194 [astro-ph.GA].
- Hoffman, Y. 2009. Gaussian Fields and Constrained Simulations of the Large-Scale Structure. In *Data analysis in cosmology*, edited by V. J. Martínez, E. Saar, E. Martínez-González, and M. -J. Pons-Bordería, 665:565–583. https://doi.org/10.1007/978-3-540-44767-2_17.
- Hoffman, Yehuda, and Erez Ribak. 1991. Constrained Realizations of Gaussian Fields: A Simple Algorithm. *The Astrophysical Journal Letters* 380 (October): L5. <https://doi.org/10.1086/186160>.
- Into, Tom, and Laura Portinari. 2013. New colour-mass-to-light relations: the role of the asymptotic giant branch phase and of interstellar dust. *MNRAS* 430, no. 4 (April): 2715–2731. <https://doi.org/10.1093/mnras/stt071>. arXiv: 1301.2178 [astro-ph.CO].
- Kafle, Prajwal R., Sanjib Sharma, Geraint F. Lewis, Aaron S. G. Robotham, and Simon P. Driver. 2018. The need for speed: escape velocity and dynamical mass measurements of the Andromeda galaxy. *MNRAS* 475, no. 3 (April): 4043–4054. <https://doi.org/10.1093/mnras/sty082>. arXiv: 1801.03949 [astro-ph.GA].
- Karachentsev, Igor, and Olga Kashibadze. 2021. Tracing the local volume galaxy halo-to-stellar mass ratio with satellite kinematics. *Astronomische Nachrichten* 342, no. 999 (August): 999–1023. <https://doi.org/10.1002/asna.20210018>. arXiv: 2109.00336 [astro-ph.GA].
- Karachentsev, Igor D., Dmitry I. Makarov, and Elena I. Kaisina. 2013. Updated nearby galaxy catalog. *The Astronomical Journal* 145, no. 4 (March): 101. <https://doi.org/10.1088/0004-6256/145/4/101>. <https://dx.doi.org/10.1088/0004-6256/145/4/101>.
- Katz, Neal, and Simon D. M. White. 1993. Hierarchical Galaxy Formation: Overmerging and the Formation of an X-Ray Cluster. *ApJ* 412 (August): 455. <https://doi.org/10.1086/172935>.
- Kim, Taehyun, Minjin Kim, Luis C. Ho, Yang A. Li, Woong-Seob Jeong, Dohyeong Kim, Yongjung Kim, et al. 2025. Accuracy of Stellar Mass-to-light Ratios of Nearby Galaxies in the Near Infrared. *AJ* 169, no. 1 (January): 44. <https://doi.org/10.3847/1538-3881/ad95eb>. arXiv: 2411.10981 [astro-ph.GA].
- Klypin, Anatoly, Gustavo Yepes, Stefan Gottlöber, Francisco Prada, and Steffen Heß. 2016. MultiDark simulations: the story of dark matter halo concentrations and density profiles. *MNRAS* 457, no. 4 (April): 4340–4359. <https://doi.org/10.1093/mnras/stw248>. arXiv: 1411.4001 [astro-ph.CO].
- Knollmann, Steffen R., and Alexander Knebe. 2009. AHF: Amiga's Halo Finder. *APJs* 182, no. 2 (June): 608–624. <https://doi.org/10.1088/0067-0049/182/2/608>. arXiv: 0904.3662 [astro-ph.CO].
- Kourkchi, Ehsan, and R. Brent Tully. 2017. Galaxy Groups Within 3500 km s⁻¹. *APJ* 843, no. 1 (July): 16. <https://doi.org/10.3847/1538-4357/aa76db>. arXiv: 1705.08068 [astro-ph.GA].
- Lelli, Federico, Stacy S. McGaugh, and James M. Schombert. 2016. SPARC: Mass Models for 175 Disk Galaxies with Spitzer Photometry and Accurate Rotation Curves. *AJ* 152, no. 6 (December): 157. <https://doi.org/10.3847/0004-6256/152/6/157>. arXiv: 1606.09251 [astro-ph.GA].
- Libeskind, Noam I., Edoardo Carlesi, Robert J. J. Grand, Arman Khalatyan, Alexander Knebe, Ruediger Pakmor, Sergey Pilipenko, et al. 2020. The HESTIA project: simulations of the Local Group. *mnras* 498, no. 2 (October): 2968–2983. <https://doi.org/10.1093/mnras/staa2541>. arXiv: 2008.04926 [astro-ph.GA].
- Libeskind, Noam I., Carlos S. Frenk, Shaun Cole, John C. Helly, Adrian Jenkins, Julio F. Navarro, and Chris Power. 2005. The distribution of satellite galaxies: the great pancake. *MNRAS* 363, no. 1 (October): 146–152. <https://doi.org/10.1111/j.1365-2966.2005.09425.x>. arXiv: astro-ph/0503400 [astro-ph].
- Libeskind, Noam I., Carlos S. Frenk, Shaun Cole, Adrian Jenkins, and John C. Helly. 2009. How common is the Milky Way-satellite system alignment? *MNRAS* 399, no. 2 (October): 550–558. <https://doi.org/10.1111/j.1365-2966.2009.15315.x>. arXiv: 0905.1696 [astro-ph.CO].
- Libeskind, Noam I., Gustavo Yepes, Alexander Knebe, Stefan Gottlöber, Yehuda Hoffman, and Steffen R. Knollmann. 2010. Constrained simulations of the Local Group: on the radial distribution of substructures. *MNRAS* 401, no. 3 (January): 1889–1897. <https://doi.org/10.1111/j.1365-2966.2009.15766.x>. arXiv: 0909.4423 [astro-ph.CO].
- Lovell, Mark R., Vincent R. Eke, Carlos S. Frenk, and Adrian Jenkins. 2011. The link between galactic satellite orbits and subhalo accretion. *MNRAS* 413, no. 4 (June): 3013–3021. <https://doi.org/10.1111/j.1365-2966.2011.18377.x>. arXiv: 1008.0484 [astro-ph.CO].
- McCall, Marshall L. 2014. A Council of Giants. *Monthly Notices of the Royal Astronomical Society* 440, no. 1 (February): 405–426. ISSN: 0035-8711. <https://doi.org/10.1093/mnras/stu199>. eprint: <https://academic.oup.com/mnras/article-pdf/440/1/405/9376493/stu199.pdf>. <https://doi.org/10.1093/mnras/stu199>.
- McGaugh, Stacy S., and James M. Schombert. 2014. Color-Mass-to-light-ratio Relations for Disk Galaxies. *AJ* 148, no. 5 (November): 77. <https://doi.org/10.1088/0004-6256/148/5/77>. arXiv: 1407.1839 [astro-ph.GA].
- Meidt, Sharon E., Eva Schinnerer, Glenn van de Ven, Dennis Zaritsky, Reynier Pletier, Johan H. Knapen, Kartik Sheth, et al. 2014. Reconstructing the Stellar Mass Distributions of Galaxies Using S⁺G IRAC 3.6 and 4.5 μ m Images. II. The Conversion from Light to Mass. *APJ* 788, no. 2 (June): 144. <https://doi.org/10.1088/0004-637X/788/2/144>. arXiv: 1402.5210 [astro-ph.GA].
- Monari, G., B. Famaey, I. Carrillo, T. Piffl, M. Steinmetz, R. F. G. Wyse, F. Anders, C. Chiappini, and K. Janßen. 2018. The escape speed curve of the Galaxy obtained from Gaia DR2 implies a heavy Milky Way. *A&A* 616 (August): L9. <https://doi.org/10.1051/0004-6361/201833748>. arXiv: 1807.04565 [astro-ph.GA].
- Müller, Oliver, Marcel S. Pawłowski, Helmut Jerjen, and Federico Lelli. 2018. A whirling plane of satellite galaxies around Centaurus challenges cold dark matter cosmology. *Science* 359 (6375): 534–537. <https://doi.org/10.1126/science.aao1858>. eprint: <https://www.science.org/doi/pdf/10.1126/science.aao1858>. <https://www.science.org/doi/abs/10.1126/science.aao1858>.
- Neuzil, Maria K, Philip Mansfield, and Andrey V Kravtsov. 2020. The Sheet of Giants: Unusual properties of the Milky Way's immediate neighbourhood. *Monthly Notices of the Royal Astronomical Society* 494, no. 2 (April): 2600–2617. ISSN: 0035-8711. <https://doi.org/10.1093/mnras/staa898>. eprint: <https://academic.oup.com/mnras/article-pdf/494/2/2600/33113646/staa898.pdf>. <https://doi.org/10.1093/mnras/staa898>.

- Olex, Edward, Alexander Knebe, Noam I. Libeskind, Dmitry I. Makarov, and Stefan Gottlöber. 2024. HINORA, a method for detecting ring-like structures in 3D point distributions I: Application to the Local Volume Galaxy catalogue. *PASA* 41 (January): e018. <https://doi.org/10.1017/pasa.2024.21>. arXiv: 2403.06187 [astro-ph.CO].
- Pawlowski, Marcel S. 2018. The planes of satellite galaxies problem, suggested solutions, and open questions. *Modern Physics Letters A* 33, no. 6 (February): 1830004. <https://doi.org/10.1142/S0217732318300045>. arXiv: 1802.02579 [astro-ph.GA].
- Peebles, P. J. E. 2023. Flat patterns in cosmic structure. *MNRAS* 526, no. 3 (December): 4490–4501. <https://doi.org/10.1093/mnras/stad3051>. arXiv: 2308.04245 [astro-ph.CO].
- Pham, Khanh, Andrey Kravtsov, and Viraj Manwadkar. 2023. Spatial and orbital planes of the Milky Way satellites: unusual but consistent with Λ CDM. *MNRAS* 520, no. 3 (April): 3937–3946. <https://doi.org/10.1093/mnras/stad335>. arXiv: 2209.02714 [astro-ph.GA].
- Pierpaoli, Elena, Stefano Borgani, Douglas Scott, and Martin White. 2003. On determining the cluster abundance normalization. *Monthly Notices of the Royal Astronomical Society* 342, no. 1 (June): 163–175. ISSN: 0035-8711. <https://doi.org/10.1046/j.1365-8711.2003.06525.x>. eprint: <https://academic.oup.com/mnras/article-pdf/342/1/163/3572367/342-1-163.pdf>. <https://doi.org/10.1046/j.1365-8711.2003.06525.x>.
- Planck Collaboration XVI. 2014. Planck 2013 results. XVI. Cosmological parameters. *A&A* 571 (November): A16. <https://doi.org/10.1051/0004-6361/201321591>. arXiv: 1303.5076 [astro-ph.CO].
- Posti, Lorenzo, and Amina Helmi. 2019. Mass and shape of the Milky Way's dark matter halo with globular clusters from Gaia and Hubble. *A&A* 621 (January): A56. <https://doi.org/10.1051/0004-6361/201833355>. arXiv: 1805.01408 [astro-ph.GA].
- Ragagnin, Antonio, Alexandro Saro, Priyanka Singh, and Klaus Dolag. 2021. Cosmology dependence of halo masses and concentrations in hydrodynamic simulations. *MNRAS* 500, no. 4 (January): 5056–5071. <https://doi.org/10.1093/mnras/staa3523>. arXiv: 2011.05345 [astro-ph.CO].
- Röck, B., A. Vazdekis, R. F. Peletier, J. H. Knapen, and J. Falcón-Barroso. 2015. Stellar population synthesis models between 2.5 and 5 μ m based on the empirical IRTF stellar library. *MNRAS* 449, no. 3 (May): 2853–2874. <https://doi.org/10.1093/mnras/stv503>. arXiv: 1505.01837 [astro-ph.GA].
- Rodríguez-Puebla, Aldo, Vladimir Avila-Reese, Xiaohu Yang, Sebastien Foucaud, Niv Drory, and Y. P. Jing. 2015. The Stellar-to-Halo Mass Relation of Local Galaxies Segregates by Color. *APJ* 799, no. 2 (February): 130. <https://doi.org/10.1088/0004-637X/799/2/130>. arXiv: 1408.5407 [astro-ph.GA].
- Rodríguez-Puebla, Aldo, Joel R. Primack, Vladimir Avila-Reese, and S. M. Faber. 2017. Constraining the galaxy–halo connection over the last 13.3 Gyr: star formation histories, galaxy mergers and structural properties. *Monthly Notices of the Royal Astronomical Society* 470, no. 1 (May): 651–687. ISSN: 0035-8711. <https://doi.org/10.1093/mnras/stx1172>. eprint: <https://academic.oup.com/mnras/article-pdf/470/1/651/17845442/stx1172.pdf>. <https://doi.org/10.1093/mnras/stx1172>.
- Rubin, Vera Cooper. 1951. Differential rotation of the inner metagalaxy. *AJ* 56 (January): 47. <https://doi.org/10.1086/106628>.
- Samuel, Jenna, Andrew Wetzel, Sierra Chapman, Erik Tollerud, Philip F. Hopkins, Michael Boylan-Kolchin, Jeremy Bailin, and Claude-André Faucher-Giguère. 2021. Planes of satellites around Milky Way/M31-mass galaxies in the FIRE simulations and comparisons with the Local Group. *MNRAS* 504, no. 1 (June): 1379–1397. <https://doi.org/10.1093/mnras/stab955>. arXiv: 2010.08571 [astro-ph.GA].
- Sawala, Till, Carlos Frenk, Jens Jasche, Peter H. Johansson, and Guilhem Lavaux. 2024. Distinct distributions of elliptical and disk galaxies across the Local Supercluster as a Λ CDM prediction. *Nature Astronomy* 8 (February): 247–255. <https://doi.org/10.1038/s41550-023-02130-6>. arXiv: 2311.00755 [astro-ph.GA].
- Shao, Shi, Marius Cautun, and Carlos S. Frenk. 2019. Evolution of galactic planes of satellites in the EAGLE simulation. *MNRAS* 488, no. 1 (September): 1166–1179. <https://doi.org/10.1093/mnras/stz1741>. arXiv: 1904.02719 [astro-ph.GA].
- Sorce, Jenny G., Stefan Gottlöber, Gustavo Yepes, Yehuda Hoffman, Helene M. Courtois, Matthias Steinmetz, R. Brent Tully, Daniel Pomarède, and Edoardo Carlesi. 2016. Cosmicflows Constrained Local UniversE Simulations. *MNRAS* 455, no. 2 (January): 2078–2090. <https://doi.org/10.1093/mnras/stv2407>. arXiv: 1510.04900 [astro-ph.CO].
- Springel, Volker, Simon D. M. White, Adrian Jenkins, Carlos S. Frenk, Naoki Yoshida, Liang Gao, Julio Navarro, et al. 2005. Simulations of the formation, evolution and clustering of galaxies and quasars. *Nature* 435, no. 7042 (June): 629–636. <https://doi.org/10.1038/nature03597>. arXiv: astro-ph/0504097 [astro-ph].
- Tamm, A., E. Tempel, P. Tenjes, O. Tihhonova, and T. Tuvikene. 2012. Stellar mass map and dark matter distribution in M 31. *A&A* 546 (October): A4. <https://doi.org/10.1051/0004-6361/201220065>. arXiv: 1208.5712 [astro-ph.CO].
- Taylor, Edward N., Andrew M. Hopkins, Ivan K. Baldry, Michael J. I. Brown, Simon P. Driver, Lee S. Kelvin, David T. Hill, et al. 2011. Galaxy And Mass Assembly (GAMA): stellar mass estimates. *MNRAS* 418, no. 3 (December): 1587–1620. <https://doi.org/10.1111/j.1365-2966.2011.19536.x>. arXiv: 1108.0635 [astro-ph.CO].
- Tully, R. Brent, Hélène M. Courtois, Andrew E. Dolphin, J. Richard Fisher, Philippe Héraudeau, Bradley A. Jacobs, Igor D. Karachentsev, et al. 2013. Cosmicflows-2: The Data. *AJ* 146, no. 4 (October): 86. <https://doi.org/10.1088/0004-6256/146/4/86>. arXiv: 1307.7213 [astro-ph.CO].
- Tully, R. Brent, Ehsan Kourkchi, Hélène M. Courtois, Gagandeep S. Anand, John P. Blakeslee, Dillon Brout, Thomas de Jaeger, et al. 2023. Cosmicflows-4. *The Astrophysical Journal* 944, no. 1 (February): 94. <https://doi.org/10.3847/1538-4357/ac94d8>. <https://dx.doi.org/10.3847/1538-4357/ac94d8>.
- Tully, R. Brent, Noam I. Libeskind, Igor D. Karachentsev, Valentina E. Karachentseva, Luca Rizzi, and Edward J. Shaya. 2015. Two Planes of Satellites in the Centaurus A Group. *ApJ* 802, no. 2 (April): L25. <https://doi.org/10.1088/2041-8205/802/2/L25>. arXiv: 1503.05599 [astro-ph.GA].
- Tully, R. Brent, Edward J. Shaya, Igor D. Karachentsev, Hélène M. Courtois, Dale D. Kocevski, Luca Rizzi, and Alan Peel. 2008. Our peculiar motion away from the local void. *The Astrophysical Journal* 676, no. 1 (March): 184. <https://doi.org/10.1086/527428>. <https://dx.doi.org/10.1086/527428>.
- Valade, Aurélien, Noam Libeskind, Daniel Pomarède, Richard Stiskalek, Yehuda Hoffman, Stefan Gottlöber, and R. Brent Tully. 2026. Constraining cosmological simulations with peculiar velocities: a forward-modeling approach. *arXiv e-prints* (February): arXiv:2602.03699. <https://doi.org/10.48550/arXiv.2602.03699>. arXiv: 2602.03699 [astro-ph.CO].
- Wang, Jie, Carlos S. Frenk, and Andrew P. Cooper. 2013. The spatial distribution of galactic satellites in the Λ cold dark matter cosmology. *MNRAS* 429, no. 2 (February): 1502–1513. <https://doi.org/10.1093/mnras/sts442>. arXiv: 1206.1340 [astro-ph.GA].
- Watkins, Laura L., Roeland P. van der Marel, Sangmo Tony Sohn, and N. Wyn Evans. 2019. Evidence for an Intermediate-mass Milky Way from Gaia DR2 Halo Globular Cluster Motions. *ApJ* 873, no. 2 (March): 118. <https://doi.org/10.3847/1538-4357/ab089f>. arXiv: 1804.11348 [astro-ph.GA].
- Weinberger, Rainer, Volker Springel, and Rüdiger Pakmor. 2020. The AREPO Public Code Release. *APJ* 248, no. 2 (June): 32. <https://doi.org/10.3847/1538-4365/ab908c>. arXiv: 1909.04667 [astro-ph.IM].

- Wempe, Ewoud, Amina Helmi, Simon D. M. White, Jens Jasche, and Guilhem Lavaux. 2025. The effect of environment on the mass assembly history of the Milky Way and M31. *arXiv e-prints* (January): arXiv:2501.08089. <https://doi.org/10.48550/arXiv.2501.08089>. arXiv: 2501.08089 [astro-ph.GA].
- Wen, Xiao-Qing, Hong Wu, Yi-Nan Zhu, Man I. Lam, Chao-Jian Wu, James Wicker, and Yong-Heng Zhao. 2013. The stellar masses of galaxies from the 3.4 μm band of the WISE All-Sky Survey. *MNRAS* 433, no. 4 (August): 2946–2957. <https://doi.org/10.1093/mnras/stt939>.
- White, M. 2001. The mass of a halo. *A&A* 367 (February): 27–32. <https://doi.org/10.1051/0004-6361:20000357>. arXiv: astro-ph/0011495 [astro-ph].
- Zaritsky, Dennis, and Helene Courtois. 2017. A dynamics-free lower bound on the mass of our Galaxy. *MNRAS* 465, no. 3 (March): 3724–3728. <https://doi.org/10.1093/mnras/stw2922>. arXiv: 1611.04574 [astro-ph.GA].
- Zaroubi, S., Y. Hoffman, K. B. Fisher, and O. Lahav. 1995. Wiener Reconstruction of the Large-Scale Structure. *ApJ* 449 (August): 446. <https://doi.org/10.1086/176070>. arXiv: astro-ph/9410080 [astro-ph].

Appendix 1. M_{200}/L_K conversion

The conversion from luminosity to halo mass in the LVG catalog is limited by the amount of information contained in this survey, which forces us to assume certain general approximations. The main inconvenience arises from the fact that LVG contains luminosity in only two bands, B and K. This limits the empirical and semi-empirical M_\star/L that can be used since only two independent variables are available. In this situation, infrared color-independent constant M_\star/L_K have traditionally been used, the best-known case being $M_\star/L_K \sim 1$ from Bell *et al.* (2003). However, this relation has the problem that it overestimates the stellar mass, so we have used other more recent estimates.

The first, (L+RP), combines M_\star/L_K expressed in the equation (1) and a semi-empirical SHMR from Rodríguez-Puebla *et al.* (2017). McGaugh and Schombert (2014) shows that in order to improve the mass estimate using infrared bands and to make it self-consistent with the estimate of other bluer bands, it is required to assume the approximately constant ratio $\log(M_\star/L) = 0.47M_\odot/L_\odot$ in $3.6\mu\text{m}$. This is equivalent to the equation (1) in the K band. Later Lelli, McGaugh, and Schombert (2016) confirms this correlation using rotation curves of nearby galaxies. Note that since the stellar mass of galaxies is determined by the different characteristics of the halo and its environment, the SHMR has a given scatter less than $\sigma_h \sim 0.15$ dex (Rodríguez-Puebla *et al.* 2015; Rodríguez-Puebla *et al.* 2017).

The second relation, (K+RP), uses M_\star/L_K obtained by infrared SED estimation of the filter with Gaussian profile centered on the central wavelength of the band K (also known as K_s), $\lambda_c = 2.16\mu\text{m}$:

$$\log(M_\star/L_K) = -0.961 + 0.073 \log(M_\star/M_\odot) \quad (9)$$

with a scatter of 0.094 dex in $\log(M_\star/L)$.

Finally, the third relation (KT) uses a direct relation between L_K and M_h , which predicts that the luminosity dependence of $\log(M_h/L_K)$ decreases for low-mass galaxies in the range $\log(L_K/L_\odot) < 9$ and increases for groups and clusters

above $\log(L_K/L_\odot) > 10.7$. Since we work with the individual luminosity of intermediate galaxies outside clusters, we will use the relation of Kourkchi and Tully (2017) corresponding to the first V-profile regime:

$$\log(M_h/L_K) = 1.5 - 0.5 \log(L_K/10^{10}L_\odot) \quad (10)$$

This relation has been tested in LVG previously in satellite kinematics derivations of the halo mass (Karachentsev and Kashibadze 2021). All $\log(M_h/L_K)$ ratios can be expressed in terms of M_{200} by means of the relation $M_h \approx 1.22M_{200}$ (White 2001; Pierpaoli *et al.* 2003).